Monthly Notices
of the
ROYAL ASTRONOMICAL SOCIETY

MNRAS **485,** L62–L67 (2019)
Advance Access publication 2019 March 7

doi:10.1093/mnrasl/slz032

The MUSE Ultra Deep Field (MUDF) – I. Discovery of a group of Lyα nebulae associated with a bright $z \approx 3.23$ quasar pair

E. Lusso [1]★ M. Fumagalli [1,2] M. Fossati [1,2] R. Mackenzie [3] R. M. Bielby,[1] F. Arrigoni Battaia,[4,5] S. Cantalupo [3] R. Cooke [1,2] S. Cristiani,[6] P. Dayal [7] V. D'Odorico,[6,8] F. Haardt,[9] E. Lofthouse,[1,2] S. Morris,[1,2] C. Peroux,[10] L. Prichard,[11] M. Rafelski,[11,12] R. Simcoe,[13] A. M. Swinbank [1] and T. Theuns[2]

[1]*Centre for Extragalactic Astronomy, Durham University, South Road, Durham DH1 3LE, UK*
[2]*Institute for Computational Cosmology, South Road, Durham DH1 3LE, UK*
[3]*Department of Physics, ETH Zurich, Wolfgang-Pauli-Strasse 27, CH-8093 Zurich, Switzerland*
[4]*European Southern Observatory, Karl-Schwarzschild-Str 2, D-85748 Garching bei Munchen, Germany*
[5]*Max-Planck-Institut fur Astrophysik, Karl-Schwarzschild-Str 1, D-85748 Garching, Germany*
[6]*INAF – Astronomical Observatory, via Tiepolo 11, I-34143 Trieste, Italy*
[7]*Kapteyn Astronomical Institute, Rijksuniversiteit Groningen, Landleven 12, NL-9717 AD Groningen, the Netherlands*
[8]*Scuola Normale Superiore, Piazza dei Cavalieri 7, I-56126 Pisa, Italy*
[9]*Dipartimento di Scienza e Alta Tecnologia, Università dell'Insubria, Via Valleggio 11, I-22100 Como, Italy*
[10]*Aix Marseille Université, CNRS, LAM (Laboratoire d'Astrophysique de Marseille) UMR 7326, F-13388 Marseille, France*
[11]*Space Telescope Science Institute, 3700 San Martin Drive, Baltimore, MD 21218, USA*
[12]*Department of Physics and Astronomy, Johns Hopkins University, Baltimore, MD 21218, USA*
[13]*MIT-Kavli Institute for Astrophysics and Space Research, 77 Massachusetts Ave. 37-664D, Cambridge, MA 02139, USA*

Accepted 2019 March 1. Received 2019 February 28; in original form 2018 December 10

ABSTRACT

We present first results from Multi Unit Spectroscopic Explorer (MUSE) observations at the Very Large Telescope in the MUSE Ultra Deep Field (MUDF), a $\approx$1.2 $\times$ 1.4 arcmin^2 region for which we are collecting $\approx$200 hours of integral field spectroscopy. The $\approx$40-h observation completed to date reveals the presence of a group of three Lyα nebulae associated with a bright quasar pair at $z \simeq 3.23$ with projected separation of $\approx$500 kpc. Two of the nebulae are physically associated with the quasars which are likely powering the Lyα emission, and extend for $\gtrsim$100 kpc at a surface brightness level of $\approx 6 \times 10^{-19}$ erg s^{-1} cm^{-2} arcsec^{-2}. A third smaller ($\approx$35 kpc) nebula lies at a velocity offset of $\approx$1550 km s^{-1}. Despite their clustered nature, the two large nebulae have properties similar to those observed in isolated quasars and exhibit no sharp decline in flux at the current depth, suggesting an even more extended distribution of gas around the quasars. We interpret the shape and the alignment of the two brighter nebulae as suggestive of the presence of an extended structure connecting the two quasar host galaxies, as seen for massive galaxies forming within gas-rich filaments in cosmological simulations.

Key words: galaxies: formation – galaxies: haloes – galaxies: high-redshift – intergalactic medium – quasars: general – large-scale structure of Universe.

1 INTRODUCTION

In the current cold dark matter (CDM) cosmological paradigm, galaxies form in overdense regions of the universe where cold ($\approx 10^4$ K) gas is accreted from the intergalactic medium (IGM) into the dark matter haloes to form stars (e.g. see Dayal & Ferrara 2018 for a recent review). As haloes assemble at the intersection of baryon-rich dark matter filaments, theory predicts the emergence of a 'cosmic web' connecting galaxies on scales of megaparsecs (Bond, Kofman & Pogosyan 1996). In the proximity of galaxies, on scales of tens to hundreds of kiloparsecs from the halo centres, these filaments are predicted to feed the circumgalactic medium (CGM), the gaseous component that is responsible for regulating the gas exchange between galaxies and the surrounding IGM (Tumlinson, Peeples & Werk 2017). This continuous refuelling of gas from filaments through the CGM, together with the ejection of baryons from haloes due to feedback processes, is believed to be the key element that regulates the growth of galaxies through cosmic time.

★ E-mail: elisabeta.lusso@durham.ac.uk

On the observational side, this theoretical framework has been explored over the past decades using absorption-line spectroscopy, which provides a powerful way to map the low-density IGM and CGM around galaxies (e.g. Steidel et al. 2010). More recently, an effective technique to map the gas distribution in the CGM has been through the direct imaging of the fluorescent Lyα line in emission around bright quasars (e.g. Cantalupo et al. 2014; Hennawi et al. 2015; Borisova et al. 2016; Arrigoni Battaia et al. 2018) and galaxies (Leclercq et al. 2017; Wisotzki et al. 2018). Instrumental to these advances has been the deployment of the Multi Unit Spectroscopic Explorer (MUSE; Bacon et al. 2010) on the Very Large Telescope (VLT).

Building on this advancement, we started a new large programme (ID 1100.A−0528; PI: Fumagalli) to collect ≈200 h of MUSE observations in a ≈1.2 × 1.4 arcmin^2 region centred at 21^h:42^m:24^s, −44°:19′:48″. Additional *Hubble Space Telescope* (*HST*) Wide Field Camera 3 (WFC3)/G141 slitless spectroscopy in the near-infrared will be collected in cycle 26 for a total of 90 orbits (PID 15637; PIs: Fumagalli and Rafelski). This field, dubbed the MUSE Ultra Deep Field (MUDF), hosts several astrophysical structures at different redshifts, including two physically associated quasars (J214225.78−442018.3 and J214222.17−441929.8) at $z \approx 3.23$, with a projected separation of ≈1 arcmin (or ≈500 kpc at $z \approx 3$). The quasar pair has ≈20 h of archival high-resolution spectroscopy and another 20 h of approved observations with Ultraviolet and Visual Echelle Spectrograph (UVES; P102A; PI: V. D'Odorico). Ultradeep MUSE observations, combined with high-resolution absorption spectroscopy of these quasars that act as bright background sources, will enable a unique view of the connection between galaxies and the IGM and CGM simultaneously in absorption and emission, extending previous studies to lower mass galaxies and lower surface brightness (SB) limits. In this first Letter,[1] we present preliminary results based on the first ≈40 h collected to date, and focus on the extended Lyα emission physically associated with the quasar pair.

2 DATA ACQUISITION AND ANALYSIS

2.1 Observations and data reduction

MUSE observations have been carried out using the Wide Field Mode with extended blue coverage[2] during the nights from 2017 August 15 up until 2018 July 18. Data were acquired in a small mosaic composed of three overlapping positions to cover both the full extent of the pair separation (62.2 ± 0.1 arcsec) and a region of ≈20 arcsec around each quasar with the ≈1 × 1 arcmin^2 field of view of MUSE (see Fig. 1). We collected a total of 102 exposures, 19 of which were obtained in 2017 August with integration times of 1200 s each, plus 83 exposures lasting 1450 s each. The total exposure time for the data presented in this Letter is therefore 39.7 h. A small dither pattern with ≈1 arcsec offsets and 10° incremental rotations has been applied to ensure optimal sampling of the field of view and to allow for better control of systematic errors associated with the uneven response across the different spectrographs. Weather conditions during the runs were on average good, with clear sky and subarcsecond seeing (≈0.6–0.8 arcsec) for the majority of the exposures. The resulting image quality, characterized by a full width at half-maximum (FWHM) = 0.60 ± 0.01 arcsec as measured across the field in the reconstructed white-light image, was enabled by the use of the GALACSI system (Stuik et al. 2006) that corrects the ground-layer turbulence across the entire field of view with four laser guide stars.

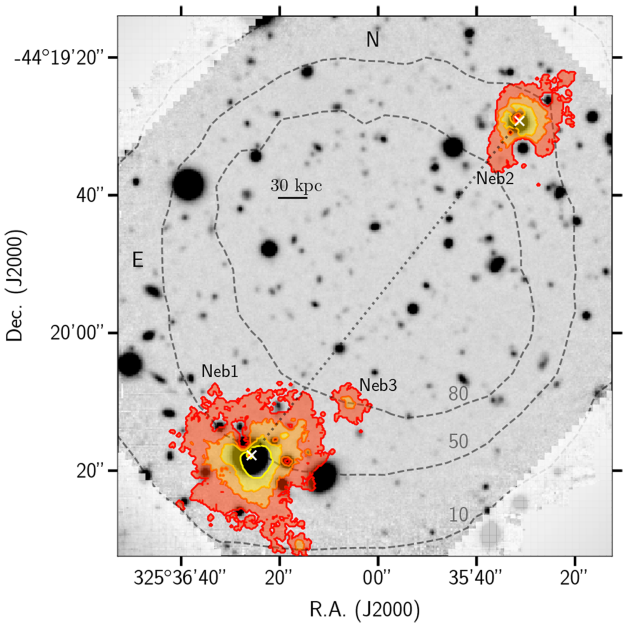

Figure 1. Optimally extracted image of the MUDF (light grey) reconstructed from the 40-h MUSE data cube. Coloured contours represent the extended Lyα emission of the three nebulae detected within ≈2000 km s^{-1} of the two quasars, with contours of surface brightness (SB) levels at 0.6, 3.2, 10, and 31.6 × 10^{-18} erg s^{-1} cm^{-2} arcsec^{-2}. The 'holes' in the nebulae are caused by the subtraction of continuum sources. The dashed lines represent the contours at 10, 50, and 80 exposures pixel^{-1} from the combined mean optimally extracted image. The alignment and morphology of these nebulae offer a tantalizing suggestion of the presence of large-scale filaments (orientation marked with a dotted line) connecting the haloes of QSO1 and QSO2 (marked with white crosses).

Observations have been reduced with the standard European Southern Observatory (ESO) pipeline (Weilbacher et al. 2014, v2.4.1) and combined in a single mosaic. We have further post-processed all the individual exposures using the CubExtractor package (v1.7; Cantalupo et al. 2019) to improve the quality of the flat-field and the sky subtraction as detailed in Borisova et al. (2016) and Fumagalli et al. (2016, 2017a). We refer the readers to these works for further details. After combining individual exposures in a final data cube using a 3σ clipping mean, we rescaled the resulting variance (which is underestimated following the resampling of pixels in the final cubes) by a wavelength-dependent factor needed to match the effective pixel root-mean-square (rms) variation in each layer.

Throughout this Letter we also use near-infrared spectroscopy available from X-SHOOTER (ESO PID 085.A−0299) for J214222.17−441929.8 (QSO2 hereafter), and that we collected using the Folded-port InfraRed Echellette (FIRE) spectrograph at the Magellan Telescope for J214225.78−442018.3 (QSO1 hereafter). The data have been reduced following the reduction techniques as discussed in e.g. López et al. (2016) and Simcoe et al. (2011). Additional details on the supporting spectroscopy available for the quasars and the adopted reduction

[1]Throughout, we adopt the following cosmological parameters: $H_0 = 70\,\mathrm{km\,s^{-1}\,Mpc^{-1}}$, $\Omega_M = 0.3$, and $\Omega_\Lambda = 0.7$. In this ΛCDM cosmology, 1 arcsec corresponds to 7.5 physical kpc.
[2]4650–9300 Å with FWHM ≃ 2.83 Å (170 km s^{-1}) at 5000 Å.

techniques will be presented in a forthcoming publication. The quasar systemic redshifts are obtained from the combined constraints provided by the broad Hβ and the narrow [O III] emission line doublet, finding $z_{\rm sys} = 3.221 \pm 0.004$ ($\sigma_z \simeq 280$ km s^{-1}) for QSO1 and $z_{\rm sys} = 3.229 \pm 0.003$ ($\sigma_z \simeq 250$ km s^{-1}) for QSO2.

2.2 Analysis of the MUSE data cube

Before proceeding to the analysis of the diffuse emission associated with the quasar pair, we post-processed the MUSE data in the following way (see Borisova et al. 2016; Fumagalli et al. 2016). The point spread function (PSF) of the quasars and of the surrounding stars was subtracted with the CubePSFSub method within CubExtractor (Cantalupo et al. 2019). We then subtracted continuum sources in the field using the CubeBKGSub procedure and ran CubExtractor on the resulting cube to search for extended Lyα emission. To this end, we focused on a slice of the cube $\pm$40 Å ($\pm$9865 km s^{-1}) on either side of the Lyα emission at the quasar redshift. In this slice, CubExtractor identified the Lyα extended emission around the quasars considering connected pixels that match the following criteria: minimum volume of 2500 connected voxels above a signal-to-noise ratio (S/N) of $\geq$2.5; a minimum area of 500 spatial pixel^2 per detection (i.e. $\sim$35 kpc on a side); and a minimum number of spectral pixels per detection of 5. We smoothed the data by 3 pixels (0.6 arcsec) using a median filter in the spatial direction only. With this selection we identified three extended Lyα nebulae, to a SB limit of $\approx 6 \times 10^{-19}$ erg s^{-1} cm^{-2} arcsec^{-2} (i.e. 4σ). For a comparison, the pixel rms at this wavelength is $\approx 1.5 \times 10^{-19}$ erg s^{-1} cm^{-2} Å^{-1} arcsec^{-2}.

The results presented in this Letter are based on the final mean cube. Our findings do not depend on the methodology of combining the data, as we find the same result using either a mean or a median. Moreover, the detection of the nebulae and their global properties is independent on the selection criteria above, as verified by performing the extraction at different S/N thresholds (i.e. 2, 3, and 5), or with different values of connected voxels (i.e. 1200, 3000) and minimum area (i.e. 400 or 600 spatial pixel^2). We have also checked that the morphology of the nebulae does not depend on the observing strategy resulting in a non-uniform exposure coverage within the field. Indeed, the analysis of the first 6 h taken with uniform exposure coverage yields a similar morphology once accounting for the different depth.

3 PROPERTIES OF THE EXTENDED NEBULAE

Our search for extended Lyα emission has uncovered the presence of three nebulae with sizes $\gtrsim$35 kpc on a side within $\approx$2000 km s^{-1} of the redshift of the two quasars. The SB maps of these nebulae, reconstructed following the method in Borisova et al. (2016) by summing the line emission along the wavelength direction inside the three-dimensional segmentation map derived by CubExtractor, are shown in Fig. 1.

3.1 Morphological properties

Nebula 1 is the most extended Lyα structure in the field, which was first identified by Arrigoni Battaia et al. (2019, ID22) with observations sensitive to $\approx 10^{-18}$ erg s^{-1} cm^{-2} arcsec^{-2}, and it is associated with the brighter quasar QSO1. With a diameter of $\approx$110 kpc measured at $\approx 10^{-18}$ erg s^{-1} cm^{-2} arcsec^{-2} and a full extent of $\approx$140 kpc measured at $\approx 6 \times 10^{-19}$ erg s^{-1} cm^{-2} arcsec^{-2}, this nebula has a total Lyα luminosity of $(6.81 \pm 0.03) \times 10^{43}$ erg s^{-1}. We also identify a second nebula, Nebula 2, that is physically associated with QSO2 and has a luminosity of $(2.52 \pm 0.02) \times 10^{43}$ erg s^{-1} and size of $\approx$50 kpc at $\approx 10^{-18}$ erg s^{-1} cm^{-2} arcsec^{-2} ($\approx$100 kpc at $\approx 6 \times 10^{-19}$ erg s^{-1} cm^{-2} arcsec^{-2}). Finally, a third nebula (Nebula 3) is identified with a velocity offset of $\approx +1550$ km s^{-1} compared to the two nebulae associated with the quasars. Smaller in size ($\approx$35 kpc at $\approx 6 \times 10^{-19}$ erg s^{-1} cm^{-2} arcsec^{-2}) and with luminosity of $(3.23 \pm 0.07) \times 10^{42}$ erg s^{-1}, this nebula is associated with a faint continuum-detected source ($m_r = 27.1 \pm 0.2$ mag), similarly to other mid-size nebulae (i.e. a few tens of kpc on a size) that are being uncovered by MUSE (e.g. Fumagalli et al. 2017b, but see also Yang et al. 2009 for similar size nebulae powered by brighter objects). A summary of the properties of the nebulae is given in Table 1.

A particularly striking feature of Fig. 1 is the relative alignment and morphology of this group of nebulae. Nebula 1 exhibits an asymmetrical shape, with a prominent arm extending to the south-west and connecting to a compact emitter. Moreover, the nebula appears to be elongated along the north-west direction, towards QSO2. Similarly, Nebula 2 is elongated along the same axis, with a clear extension pointing back towards Nebula 1.

To quantify the elongation, we compute the asymmetry parameter α (the ratio between the semiminor and semimajor axis) and the position angle describing the light distribution Φ as in Arrigoni Battaia et al. (2019), finding $\alpha \approx 0.80$ and $\Phi \approx -56.^{\circ}8$ for Nebula 1 and $\alpha \approx 0.91$ and $\Phi \approx -48.^{\circ}1$ for the Nebula 2. Within uncertainties (see Arrigoni Battaia et al. 2019 for details), the similar Φ values for both nebulae provide an additional indication of alignment along a common axis for these systems. Moreover, the probability of the nebulae to be randomly oriented can be estimated as the ratio between the subtended angle of the nebulae ($\approx 50^{\circ}$) and 2π $(50/360)^2$, which is only 2 per cent. The alignment of the nebulae thus likely reflects the presence of an underlying structure not currently detected.

While not at the exact same redshift ($z \simeq 3.25$), Nebula 3 lies in between the two quasars, again aligned in projection with the axis connecting QSO1 and QSO2. Altogether, these features are suggestive of the presence of filamentary structures extending from the haloes of the two host galaxies. These elongated nebulae, which appear to be a scaled-up version of what is inferred from the stacking of MUSE observations of pairs of Lyα emitters (Gallego et al. 2018), are thus hinting at the presence of a filament connecting the nodes where haloes form. From a theoretical perspective, this picture is consistent with the structures predicted in cosmological hydrodynamic simulations (e.g. Fumagalli et al. 2011; Rosdahl & Blaizot 2012; van de Voort et al. 2012; Schaye et al. 2015). Our results, albeit on larger scale, are also comparable to the much extended Lyα nebula discovered in a quasar pair at $z = 2.4$ by Cai et al. (2018). With a projected separation of only $\approx$80 kpc, this pair is powering a common nebula with a size of $\approx$232 kpc featuring an elongated morphology along the line connecting the two quasars in projection.

Despite being clustered within a $\approx$500 kpc region on a side, Nebulae 1 and 2 lie within the parameter space defined by single quasars of comparable magnitude at these redshifts. In particular, they exhibit typical sizes and Lyα luminosities (see e.g. fig. 3 in Borisova et al. 2016 and fig. 15 in Arrigoni Battaia et al. 2019). This suggests that quasar nebulae trace halo gas within their host galaxies and that their clustered nature is a consequence of the

Table 1. Global properties of the three Lyα nebulae.

Object	$z_{\rm neb\,Ly\alpha}$	$z_{\rm qso}$	m_r^a	FWHM$^b_{\rm Ly\alpha}$ (km s^{-1})	$F_{\rm Ly\alpha}$ (10^{-18} erg s^{-1} cm^{-2})	$L_{\rm Ly\alpha}$ (10^{43} erg s^{-1})	Size^c (kpc)
Neb1	3.230	3.221 ± 0.004	17.9 ± 0.02	1124 ± 23	748.9 ± 3.5	6.81 ± 0.03	140
Neb2	3.229	3.229 ± 0.003	20.5 ± 0.03	1153 ± 24	276.7 ± 1.8	2.52 ± 0.02	100
Neb3	3.254	–	27.1 ± 0.20	513 ± 25	35.5 ± 0.6	0.32 ± 0.01	35

^{a}Continuum AB magnitudes at $\lambda = 6184.27$ Å, convoluted with the Sloan Digital Sky Survey (SDSS) $r*$ filter and corrected for Galactic extinction, for the two quasars and the counterpart of Nebula 3. ^{b}Full width at half-maximum of the narrow Lyα emission line. ^{c}Approximate size of the nebula at 6×10^{-19} erg s^{-1} cm^{-2} arcsec^{-2}.

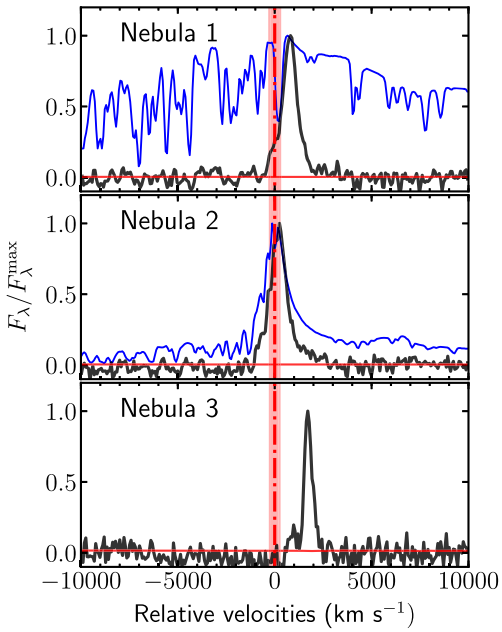

Figure 2. MUSE spectra of the QSO1 and QSO2 (blue lines) and of the associated nebulae (black lines with related uncertainties in red) at the location of the Lyα emission. Velocities are relative to the systemic redshift of the quasars, whilst the average redshift of 3.23 is assumed as a reference for Nebula 3. Fluxes are normalized to their peak in this wavelength range.

distribution of haloes in CDM. Indeed, the expectation is that the 'isolated' nebulae reported in the literature are themselves clustered with Lyα nebulae that are just below the SB level reached by shallower observations in quasar fields (see e.g. Wisotzki et al. 2018).

3.2 Spectral properties

In Fig. 2, we present the spectra extracted from the MUSE cube for QSO1 and QSO2 and the associated nebulae at the location of the Lyα emission, shown in velocity space relative to the quasar systemic redshift. The spectra are extracted using pixels that spatially overlap with the CubExtractor segmentation map, after we have masked out all the continuum sources detectable in the white-light image reconstructed from the MUSE cube. Fluxes are then normalized at the Lyα flux peak emission. As found by Borisova et al. (2016) and Arrigoni Battaia et al. (2019), the extended Lyα emission is characterized by a much narrower line profile than the broad Lyα emission of the quasars. This is expected for gas that traces material within the galaxy halo, outside the black hole sphere of influence. Nebula 1 also displays a small shift of $\approx$600 km s^{-1} with respect to the quasar redshift, an offset that has been also found in previous works (e.g. Arrigoni Battaia et al. 2019). As deeper data becomes available, it will be possible to investigate in more detail the spatially resolved kinematics of the nebulae, in connection with the quasar spectral properties.

The Lyα in Nebula 3 is displaced by a velocity offset of $\approx +1550$ km s^{-1} compared to Nebula 1 ($\approx +2200$ km s^{-1} compared to the systemic redshift). Considering the velocity offset as an upper limit to the Hubble flow velocity, Nebula 3 lies at < 5 Mpc (proper) and hence it is likely to be associated with the same large-scale structure hosting the quasars and within the region influenced by the quasars' radiation field (Cantalupo et al. 2014). With a line FWHM of 513 ± 25 km s^{-1} this nebula is presumably powered by an obscured active galactic nucleus (AGN), making it quite likely that several AGNs coexist within this structure, as seen for instance in the nebula discovered by Hennawi et al. (2015), Arrigoni Battaia et al. (2018), and Cai et al. (2017, see also Husemann et al. 2018a,b). This hypothesis can be tested with future X-ray observations.

3.3 Surface brightness profiles

As a final step, we derived the Lyα surface brightness (SB) profiles for Nebula 1 and Nebula 2 within the two pseudo-slits shown in Fig. 3 along the direction of the expected filament connecting the two haloes. For this calculation, we relied on narrow-band images of $\pm$15 Å ($\pm$ 3700 km s^{-1}) reconstructed around the Lyα line centre of each nebula after subtracting continuum-detected sources from the data cube. The use of a narrow-band image is preferable over the optimally extracted map as it conserves flux. To derive the profile, we average the flux in boxes of $\approx$34 pixels along the pseudo-slit, propagating the error accordingly. As the formal error does not account for the pixel covariance, we also calculate an empirical detection limit of $\approx 2.4 \times 10^{-19}$ erg s^{-1} cm^{-2} arcsec^{-2} on the SB from the distribution of fluxes calculated along $\approx$1000 apertures of $\approx$34 pixels located randomly in the field and shown as a green dashed line in Fig. 3. This analysis highlights the different extents of the Lyα emission around the quasars. In particular, Nebula 1 displays a clear excess of emission at $\simeq$50 kpc from the centre towards the direction of the expected filament. This excess, albeit less pronounced, may also be present in the Nebula 2.

When compared to the detection limit for line emission, it is evident that the SB profiles show no marked truncation radius (especially for the brighter Nebula 1, see right-hand panel of Fig. 3) up to the current detection level. A reconstruction of the underlying gas distribution from the observed profile is not straightforward due to Lyα radiative transfer effects and uncertainties in the mechanisms that power the emission (e.g. Cantalupo et al. 2014; Gronke & Bird 2017). However, at face value, the absence of a sharp decline in flux implies the presence of halo gas on scales larger than probed by current observations (Prochaska et al. 2013). Upcoming deeper

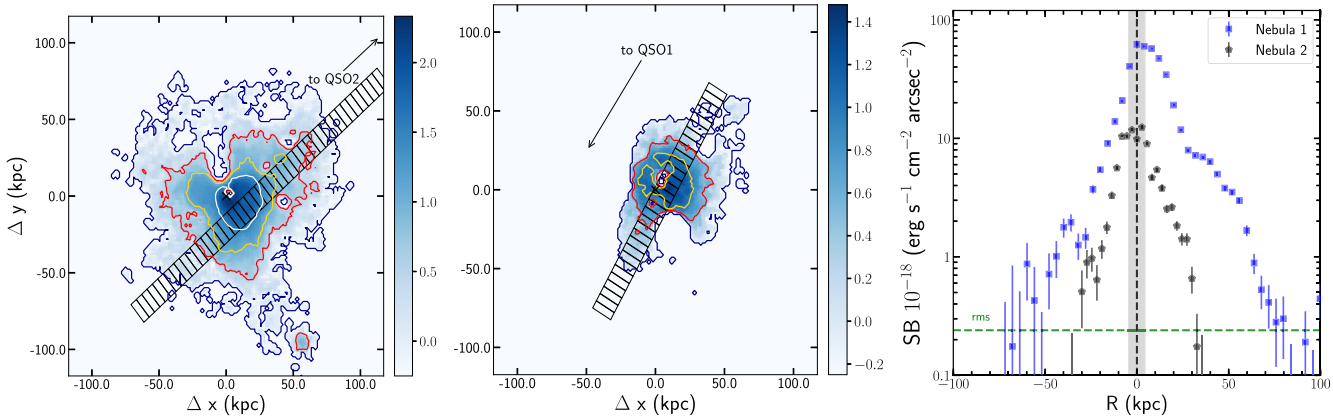

Figure 3. Lyα SB maps for Nebula 1 associated with QSO1 (left-hand panel) and Nebula 2 associated with QSO2 (central panel) with contours at 0.6, 3.2, 10, and 31.6 $\times$ 10^{-18} erg s^{-1} cm^{-2} arcsec^{-2} in blue, red, yellow, and white, respectively. The pseudo-long slits utilized to calculate the radial profiles are also shown. Right-hand panel: SB radial profiles extracted along pseudo-slits in the direction of the expected filament connecting the two quasars computed from the narrow-band images. Also shown (green dashed line) is the empirical rms of $\simeq$2.4 $\times$ 10^{-19} erg s^{-1} cm^{-2} arcsec^{-2}. The grey shaded area marks the average full width at half-maximum (FWHM) of the point spread function (PSF) estimated from stars within the field ($\approx$4.5 kpc at $z \simeq 3.23$). For clarity purpose, data below rms/2 are not shown.

observations in the MUDF will probe this gas distribution and the putative filament at larger distances from the host galaxies.

4 CONCLUSIONS

We presented preliminary results from $\approx$40 h of observations in the MUDF, a 1.2 $\times$ 1.4 arcmin^2 sky region at 21^h:42^m:24^s, $-$44°:19′:48″ that will be observed for a total of $\approx$200 h with MUSE, plus 90 orbits with the WFC3 G141 grism on board of *HST*. With the $\approx$40 h of observations collected to date, we studied the extended Lyα emission associated with a bright quasar pair at $z \approx 3.23$ with a projected separation of 500 kpc. Our primary findings are the following.

We detected two extended Lyα nebulae, physically associated with the two quasars (QSO1 and QSO2), with sizes of $\approx$140 and $\approx$50 kpc measured at 6 $\times$ 10^{-19} erg s^{-1} cm^{-2} arcsec^{-2}. The two nebulae have Lyα luminosities of $\approx$7 $\times$ 10^{43} and 2.5 $\times$ 10^{43} erg s^{-1}, respectively. A third nebula is detected close to quasar QSO1 in projection, but at a velocity offset of $\approx$1550 km s^{-1}. The three nebulae are believed to trace gas in haloes clustered in the same large-scale structure.

Despite their clustered nature, the two quasar nebulae have global properties (e.g. size and luminosity) in line with what found for isolated nebulae. However, their alignment and elongated morphology is suggestive of one or more gas filaments connecting the quasar host galaxies, as predicted by cosmological simulations.

After extracting SB profiles along pseudo-slits in the direction of the putative filament, we confirm that these nebulae present asymmetric profiles along the line connecting the quasars. At the depth of our observations, we do not identify sharp edges, implying the presence of even more extended halo gas.

Upcoming observations in MUDF will enable a deeper view of the possible filament between the quasar pair, as well as of other structures that lie in the MUDF footprint at different redshifts.

ACKNOWLEDGEMENTS

We thank the anonymous reviewer for useful comments. EL is supported by a European Union COFUND/Durham Junior Research Fellowship (grant agreement no. 609412). We acknowledge support by the Science and Technology Facilities Council [grant number ST/P000541/1] and from the European Research Council under the European Union's Horizon 2020 research and innovation programme (grant agreement nos. 717001 and 757535). This Letter is based on observations collected at ESO/VLT (ID 1100.A-0528). SC gratefully acknowledges support from Swiss National Science Foundation grant PP00P2_163824. RC was supported by a Royal Society University Research Fellowship.

REFERENCES

Arrigoni Battaia F., Prochaska J. X., Hennawi J. F., Obreja A., Buck T., Cantalupo S., Dutton A. A., Macciò A. V., 2018, MNRAS, 473, 3907
Arrigoni Battaia F., Hennawi J. F., Prochaska J. X., Oñorbe J., Farina E. P., Cantalupo S., Lusso E., 2019, MNRAS, 482, 3162
Bacon R. et al., 2010, Proc. SPIE, 7735, 773508
Bond J. R., Kofman L., Pogosyan D., 1996, Nature, 380, 603
Borisova E. et al., 2016, ApJ, 831, 39
Cai Z. et al., 2017, ApJ, 837, 71
Cai Z. et al., 2018, ApJ, 861, L3
Cantalupo S., Arrigoni-Battaia F., Prochaska J. X., Hennawi J. F., Madau P., 2014, Nature, 506, 63
Cantalupo S. et al., 2019, MNRAS, 483, 5188
Dayal P., Ferrara A., 2018, Phys. Rep., 780, 1
Fumagalli M., Prochaska J. X., Kasen D., Dekel A., Ceverino D., Primack J. R., 2011, MNRAS, 418, 1796
Fumagalli M., Cantalupo S., Dekel A., Morris S. L., O'Meara J. M., Prochaska J. X., Theuns T., 2016, MNRAS, 462, 1978
Fumagalli M., Haardt F., Theuns T., Morris S. L., Cantalupo S., Madau P., Fossati M., 2017a, MNRAS, 467, 4802
Fumagalli M. et al., 2017b, MNRAS, 471, 3686
Gallego S. G. et al., 2018, MNRAS, 475, 3854
Gronke M., Bird S., 2017, ApJ, 835, 207
Hennawi J. F., Prochaska J. X., Cantalupo S., Arrigoni-Battaia F., 2015, Science, 348, 779
Husemann B., Worseck G., Arrigoni Battaia F., Shanks T., 2018a, A&A, 610, L7

Husemann B., Bielby R., Jahnke K., Arrigoni-Battaia F., Worseck G., Shanks T., Wardlow J., Scholtz J., 2018b, A&A, 614, L2
Leclercq F. et al., 2017, A&A, 608, A8
López S. et al., 2016, A&A, 594, A91
Prochaska J. X. et al., 2013, ApJ, 776, 136
Rosdahl J., Blaizot J., 2012, MNRAS, 423, 344
Schaye J. et al., 2015, MNRAS, 446, 521
Simcoe R. A. et al., 2011, ApJ, 743, 21
Steidel C. C., Erb D. K., Shapley A. E., Pettini M., Reddy N., Bogosavljević M., Rudie G. C., Rakic O., 2010, ApJ, 717, 289
Stuik R., Bacon R., Conzelmann R., Delabre B., Fedrigo E., Hubin N., Le Louarn M., Ströbele S., 2006, New Astron. Rev., 49, 618
Tumlinson J., Peeples M. S., Werk J. K., 2017, ARA&A, 55, 389
van de Voort F., Schaye J., Altay G., Theuns T., 2012, MNRAS, 421, 2809
Weilbacher P. M., Streicher O., Urrutia T., Pécontal-Rousset A., Jarno A., Bacon R., 2014, in Manset N., Forshay P., eds, ASP Conf. Ser. Vol. 485, Astronomical Data Analysis Software and Systems XXIII. Astron. Soc. Pac., San Francisco, p. 451
Wisotzki L. et al., 2018, Nature, 562, 229
Yang Y., Zabludoff A., Tremonti C., Eisenstein D., Davé R., 2009, ApJ, 693, 1579

This paper has been typeset from a TEX/LATEX file prepared by the author.